Hindawi
Journal of Nanomaterials
Volume 2022, Article ID 7957007, 19 pages
https://doi.org/10.1155/2022/7957007

Review Article

Role of Phytonanotechnology in the Removal of Water Contamination

Apurva Gole,[1] Diya John,[1] Karan Krishnamoorthy,[1] Nilesh S. Wagh,[1] Jaya Lakkakula,[1,2] Mohd Shahnawaz Khan,[3] Hamza Ahmad Mohammad Odeibat,[3] Mohammad Tarique,[4] and Md. Rabiul Islam[5]

[1]*Amity Institute of Biotechnology, Amity University Maharashtra, Mumbai-Pune Expressway, Bhatan, Panvel, Mumbai, Maharashtra 410206, India*
[2]*Centre for Computational Biology and Translational Research, Amity Institute of Biotechnology, Amity University Maharashtra, Mumbai- Pune Expressway, Bhatan, Panvel, Mumbai, Maharashtra 410206, India*
[3]*Department of Biochemistry, College of Sciences, King Saud University, Riyadh, Saudi Arabia*
[4]*Department of Child Health, School of Medicine, University of Missouri, Columbia, Missouri 65201, USA*
[5]*Department of Pharmacy, University of Asia Pacific, Dhaka, Bangladesh*

Correspondence should be addressed to Nilesh S. Wagh; waghnil@gmail.com, Jaya Lakkakula; spencerjaya@gmail.com, and Md. Rabiul Islam; robi.ayaan@gmail.com

Received 20 February 2022; Accepted 7 March 2022; Published 29 March 2022

Academic Editor: Palanivel Velmurugan

Environmental pollution is expedited by the rapid increase in population, urbanization, industrialization, and growth in the global economy. Water contamination is accelerated by the incautious disposal of wastes into water bodies. The need of the hour is to develop novel, ergonomic, subsidized, and reproducible technologies that assist in the remediation of such wastes that require minimal human intervention, preserve the quality of water, and are eco-friendly. Phytonanotechnology is emerging as a promising strategy, characterized by the biosynthesis of metallic nanomaterials and nanoparticles (NPs) using plant-based sources. Conventional remediation technologies like adsorptive, reactive, in situ, ex situ, and open fabrication of phytogenic magnetic NPs (PMNPs) have already been established in scientific literature. A keen understanding of building material platforms, fabricating and performance-optimizing are required to develop nanomaterials capable of addressing environmental issues. Furthermore, their antimicrobial activity, biodegradability and biocompatibility, optoelectronic properties, low toxicity, availability, energy efficiency, and versatility have been utilized efficiently.

1. Introduction

Over the last few years, an increasing number of nanomaterials have been developed specifically for environmental applications, and they have been used to remediate contaminated soil and groundwater from hazardous waste present in them. The materials used for the remediation of pollutants are to be ensured that they do not become pollutants after being implemented. Thus, biodegradable materials are an excellent choice for the application. Biodegradable materials offer an eco-friendly and safer alternative for the effective treatment of pollutants while increasing the rate of acceptance of modern technology [1].

A high surface area-to-volume ratio coupled with remarkable reactive sites contribute to the high reactivity of nanomaterials. Low efficiencies derived from off-targeting are nullified using new technologies which rely on target-specific capture of contaminants. Surfaces of nanoengineered materials which are modified through physical and chemical methods serve to combat the challenges faced in removal of water contamination. NPs offer appealing features such as biodegradability, nontoxicity, cost-effective synthesis and

maintenance, target-specific capture, recyclability, and the potential for recovery after use, which supports their extensive use despite demerits that include recovery costs, toxicity of metallic NPs and their by-products, and requirement of special preparation techniques owing to their limited stability under normal conditions [2].

Nanomaterials should be developed with a thorough comprehension of the fabrication processes, performance optimization strategies, and material platforms. Long term, this approach could assist us in addressing environmental issues on a larger scale. Extracts obtained from different parts of plants naturally act as capping agent, and this property can be exploited to synthesize metallic NPs under Phytonanotechnology [3].

Phytonanotechnology is a discipline that governs the use of plant-based or plant-mediated biomaterials in the synthesis of metallic NPs for the detection of lethal pathogens in those facilities and to assess the degree of risk imposed by other factors to the environment. The infallibility and eco-friendliness of these processes have contributed to its industrial usage [4].

Lead has been depended on for various industrial purposes that has resulted in large-scale water contamination and significant health hazards in many parts of the world. Biologically synthesized magnetic NPs of iron oxide (II, III) (Fe_3O_4) were designed for the removal of metal from a solution (aqueous). The leaf extract of *Moringa oleifera* was specifically used and confirmed the size of the NP in the range of 60-100 nm. The synthesized NPs achieved 94.08% removal of lead within 60 min of contact time [5].

Cobalt oxide NPs have been reported to be eco-friendly, facile, nontoxic, and highly resistant to corrosion and oxidation. The NPs were synthesized using the fruit extract of *Vitis rotundifolia* using coprecipitation. With a reaction time of 150 min and a degradation potential of 98%, the acid blue 74 dye was chosen as a standard for the measurement of photocatalytic activity of the NPs [6].

There are continuous efforts in research to develop NPs from different sources. An emerging branch of nanotechnology seeks to synthesize NPs from natural sources such as bacteria and fungi. The green synthesis of such NPs relies on secondary metabolite extracts, the mycelial surface of fungi, and bacterial culture growth rate extracts of the plant which are the main accessible mechanisms in synthesis. The topography of the land area also demands the action of appropriate in situ and ex situ technologies. In situ remediation can reach inaccessible areas such as crevices and aquifers which eliminates the need for other expensive operations [7].

The main objective of this review is to understand how Phytonanotechnology is utilized in the bioremediation of wastewater. The content pertains exclusively to bioremediation of pathogens, organic compounds, dyes, and heavy metals (Figure 1).

2. Role of Phytonanotechnology in Removal of Water Contamination

A pioneering approach in response to the growing concern of water contamination is the utility of green synthesized nanomaterials which possess superior chemical reactivity, greater mechanical durability, higher surface area-to-volume ratio, and absorption-adsorption potentials which facilitate the removal of effluents along the lines of heavy metals, organic compounds, dyes, and pathogens discharged consequently as a ramification of domestic, commercial, and industrial activities. The upcoming sections engage each of these categories centrally and focus on the commission of novel methods and biomaterials for their removal from such resources or reservoirs.

2.1. Role of Phytonanotechnology for Removal of Heavy Metals. Different industries release effluents in the form of toxic heavy metals which find applications in research labs and in production plants, into wastewater. The prominent use of these metals in a wide range has been a cause of water pollution, and it is increasing at a rapid rate. Many metals like chromium, arsenic, copper, iron, and cadmium are found in water bodies.

Iron NPs were prepared from *barberry* leaves extract, and a ferric chloride solution of 0.1 M was prepared. Weight percentages of carbon and oxygen were obtained as 48.4 and 44.5% (estimate), respectively, *via* EDS, and its map scanning shows uniform distribution of Fe and Cr. The elemental speciation of GT-nFe surfaces and its mapping prior to Cr removal and after was expedited using XPS, which showed peak results at 712.4, 719.1, and 726.1 eV, assigned to Fe 2p3/2, Fe0, and Fe 2p1/2, sequentially. The acidic pH condition gives high efficiency of Cr removal by the NPs with the rate of 99.7% at a pH of 4 within 6 h along with the dosage of 0.5 g/l −0.12 g/l in acidic conditions. The 100% removal of Cr went down to 17.7% when the initial concentrations of Cr were increased to 200 mg l^{-1}. With higher temperature, there was high absorbance and the isotherm models of Freundlich and Langmuir were employed which described the Cr (VI) adsorption [8].

The NPs obtained from *Konjac glucomannan* were at a size range of 5.98 ± 2.02 nm, and to detect the presence of metal particles, EDS was employed along with Pd NPs with 3.0 keV as a strong peak. The EDS mapping also determined the elemental composition of NPs. The Pd NPs had a size range of 3.2 to 10.0 nm and was confirmed via DLS, and the XRD spectra showed the crystalline structure. TEM analysis shows the particles as spherical and worm-like shapes. During the removal of Cr, the absorption peak was seen at 350 nm which was estimated because of the LMCT with an overall of 93% of Cr reduction at 45°C along with Azo dyes reduction; the entire mechanism followed the pseudo-first-order [9].

Green tea leaf extracts were used for the preparation of Fe-NPs, and those were implemented for the Cr removal from the wastewater. The SEM results showed that the NPs have an irregular spherical shape with a diameter of range 30 to 100 nm in size. The before and after reaction results of XPS spectra showed that GT-nFe exhibited characteristic peaks after exposure to Cr. Higher removal efficiencies were found in acidic medium and high temperatures, and 100% removal efficiency was attained with the dosage of 0.12 g l^{-1} but with limited presence of Cr (VI) concentration and mechanism [10].

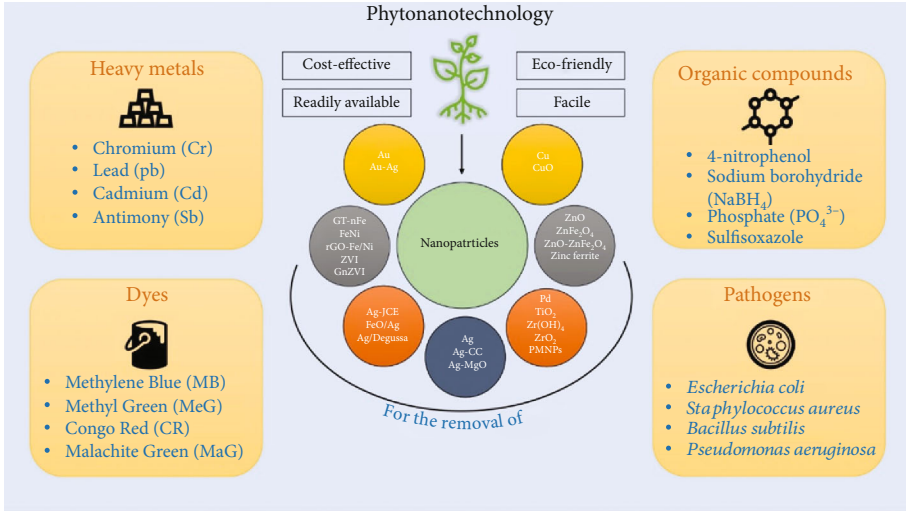

Figure 1: Graphical abstract depicting the application of Phytonanotechnology in the removal of wastewater contaminants.

The removal of chromium was achieved using iron NPs harnessed from straw waste powder. They were dried at 80°C forming a solid powder, and the precursor was incubated in a nitrogen atmosphere for 120 min at 800°C for calcination and obtaining hierarchically porous carbon (HPC) by heating them at the rate of 3°C $min^{-1.}$ Similarly, most of the NPs were prepared and applied with the use of heat, biomaterial, and radiations. SEM analysis gave the morphological analysis of the NPs, and in the reactivity test, Ni doping results to the increase in Cr removal. The higher dosage did not favor the removal capacity of NPs, 0.5 g L^{-1} is the optimized dosage. The maximum removal efficiency was 99.7% in 4 h [11].

A fresh banana waste peduncle (BWP) was obtained, and spherical AgNPs 25 nm in size on average as per TEM images were fabricated which facilitated Cr removal. The absorption peak was seen at 3453 cm^{-1} *via* FTIR for BWP extract. The photoreduction of Cr(VI) was monitored by the decay around 350 nm and was reduced by a minimal amount of 9% but increased with the presence of strong oxidants, and the same NPs were also effective for the removal of MB dye and Cr along with antimicrobial activity [12].

Similarly, petroleum wastewater has contaminants like Cr and Cd; and Ag-NPs are synthesized from the walnut fruit for its remediation. The NPs average size was 47.4nm which was estimated via TEM. They also showed a round shape without any aggregation with 41.2eV of zeta potential conforming a negative charge of NPs. The absorption increased along with the increase in temperature until 35°C and no further change above it. The total absorption capacity was seen as 81.3% for Cr and 88.1% for Cd ions when petroleum wastewater was used. At pH2, photocatalytic reduction of Cr was observed at full absorption potential and followed pseudo-second order model of kinetics [13].

Silver NPs were also obtained from *Benjamina* leaves extract termed as *Ficus benjamina* leaves extract (FBLE). A formula as %removal = ¥ Co – Ce/Co ∗ 100 was used to estimate the total removal of Cd (II) from polluted water. The presence of proteins and polyphenols was confirmed by FTIR spectral images. Different concentrations and conditions were considered, and the highest Cd (II) removal % was recorded at 40 min, and the SEM results showed that the Ag-NPs have a dendritic structure [14].

Green tea extracts were also used for the removal of Sb contaminants, and the NPs had a smooth surface which was seen and observed via SEM. The BET analysis showed the pore-like structure of NPs which were in a range of 10–100nm. The removal efficiency of Sb decreased from 66.5 to 36.8% with the increase in the Sb contaminants in the solution from 0.5 to 2 mg l^{-1} but also increased with an increase in pH, along with the GO-Fe/Ni dose and temperature. The pseudo-first-level model of kinetics best explained the oxidation of Sb(III) to Sb(V) [15].

Rice residue powder was used for the removal of arsenic, and the biochar obtained from it was labelled as MBC (magnetic biochar) of which 10 g was later added to ethanol-water solution (60%, v/v) and to 2 ml of ammonia (28%). ZBC were obtained when a solution of $ZrOCl_2.8H_2O$ was added to the entire solution and left at RT for 24 h. Both MBC and ZBC were at a size of 200nm. Their crystalline structures were obtained by use of XRD. After the introduction of the NPs in the MBC, the capacity for As removal was observed to be increased; also, the SBET showed that ZBC had a more porous structure than MBC. Even zero-valent iron NPs (ZVI NPs) are gaining huge demand in the water remediation methods because of their characterization of heavy metal removal. It also possesses some antimicrobacterial properties [16].

Black tea (BT) was prepared by heating tea powder in distilled water, and the extract was later vacuum-filtered. $FeSO_4$ solution with 0.1 molarity was added to the extract at a ratio of 1 : 2. The polyphenol groups present act as reducing and capping agents by forming complexes with Fe metal ions producing zero-valent metals which forms ZVI NPs which were then later collected by using vacuum filtration. In the ongoing work, we modify the efficiency NPs by using gamma radiation and its effects on the structural properties of NPs, and hence, the removal efficiency

of Cu^{2+} ions goes up to 97% at pH 5. The removal efficiency decreased linearly with an increasing temperature which is a typical behavior for exothermic adsorption processes. The absorbent is relatively stable as the removal capacity was 85% even after six regeneration cycles. The NPs also possess antibacterial activity which was effective against *S. coccus*, *S. aureus*, and *E. coli* [17].

Similarly, *Ziziphus jujuba* leaves extract was used to obtain zinc oxide NPs which were used for the removal of Pb and dyes like MO and MB by absorption mechanism. The absorption peaks at 3421 cm^{-1}, 2925 cm^{-1}, 1637 cm^{-1}, and 1384 cm^{-1} (3421 cm^{-1} was strongest) using FTIR were observed, whereas Bragg's reflection using XRD for ZnO NPs were recorded at $2\theta = 31.73°$, 34.38°, and 36.20 with an average of 15 nm NPs as obtained from TEM. ZnO NPs because of their small particle sizes and overall high surface area decreased the removal efficiency when contrasted with G ZnO NPs. GMW ZnO NPs rapidly removed all toxins present within the sample in 30 min, pH 5.6 at 25°C [18].

Silver NPs were obtained using *Piliostigma thonningii* leaf extract. Time, pH, temperature, and total $AgNO_3$ content were maintained in a controlled environment to obtain the contaminants' removal efficiencies. An absorbance maximum was observed at 415 nm when incubated for 60 min at an optimum pH of 6.5 and temperature of 65°C, and the concentration of $AgNO_3$ was 1.25 mM. The NPs were spherical with a size range of 50–114 nm with a crystalline structure. The elemental synthesis of sliver was at 2.60 keV which was confirmed by EDX, and the capping agent was suggested to be hydroxyl (OH) group. The NPs also showed heavy metal removal activity in laboratory simulated wastewater [19].

Simarouba glauca leaf extract was used to obtain copper ferrite NPs for Pb removal. These metal oxide NPs are very cost-efficient as they can be recovered at the end of the reaction and can be reused up to 3 times and also possess antimicrobial properties. The average crystallite size of $CuFe_2O_4$ is 9 nm which was confirmed by XRD. The absorption mechanism was observed with different dosage levels from 0.025 g to 0.1 g/100 ml in 10 mg/l lead solution, and the analysis showed that after a certain dosage, there was no increase in absorption at pH 6 with 80% Pb removal efficiency [20].

In another work, Au-NPs with particle size between 22 and 54 nm were synthesized using a reducing sample of lemon juice extract. FTIR results indicate the electrostatic interaction between Au-NPs and oxygen atoms in C=O due to the lone pairs. Even though the main study focused on nickel removal, the results showed 100% remediation for Pb. These NPs were used on Wilkerson Filters to confirm the results [21].

Dried seed extracts of *Moringa oleifera* is used to synthesize Fe-NPs for Pb(II) removal from water. Varied concentrations of the NPs showed different removal efficiencies for different contaminants; for the removal of heavy metals like zinc, scandium, silver, lead, and mercury, the precipitate was formed in 30 min. The optimized amount for the experiment was 0.5 mM $AgNO_3$ and the SEM image showed that the NPs are of size 4 nm with an even shape and spherical surface. The AFM results showed that the NPs have different sizes and a crystalline structure was observed from XRD and TGA results [22].

2.2. Role of Phytonanotechnology for Removal of Organic Compounds. Triclosan (TCS) is an organic compound that is a huge threat as a water pollutant and can cause various health diseases. Bimetallic iron/nickel NPs were used for the removal of the same. A solution of dried 30 g *eucalyptus* leaves and 500 ml of deionized water was prepared with 1 h incubation at 80°C. The extract obtained was filtered, and reagents were added; later, the suspension was vacuum filtered, rinsed with ethanol, and freeze-dried. In the experiment along with the TCS, the Cu removal was also achieved. The sample was taken in amber centrifuges and was added with Fe/Ni NPs and filtered using 0.22 μm PTFE membrane filters. With the following formula $R\% = C_0 - C_t / C_0 * 100$, the removal efficiency was calculated. SEM determined that the average size of NPs was polydisperse (60–85 nm) before reaction and was increased slightly after the reaction with TCS and Cu, and the EDS spectrum depicted the change in contents of Fe from 11.8% to 15.4% and Ni from 0.7% to 0.4%. FTIR spectra showed that the attributable characters were at peak and retained in the entire reaction. The XPS analysis showed that the NPs became more corroded after exposure to the contaminants. The mix contaminant removal was higher than the single contaminant removal rate with a constant pH at 6, and with higher dosage of NPs, the Cu removal is increased. The optimal removal was at 30°C [23].

The leaf extract was prepared from *Ipomoea carnea* leaves with dry seeds of *Brassica alba* which were both powdered. Both the seed powder and the leaf extract were each boiled in 100 ml of deionized sterile water for 60 min, and the NP obtained from this extract was used to remove an organic compound, chlorfenapyr, from the water. The NPs could be cubical, circular, triangular, hexagonal, or rod-shaped, with a size range of 6.27–21.23 nm. The crystalline structure was observed via SAED. When some other NPs like Ip–Ag0, F–Fe0, and Br–Ag0 are present, the chlorfenapyr binds to them enhancing the process of degradation. With the help of these extra NPs presence, the removal efficiencies were seen as 73.10% for Br–Ag0, with 71.22% for F–Fe0, and 57.32% for Ip–Ag0. In the flooded soil water, the efficiency was observed to be 25.83%, and the chlorfenapyr was removed more efficiently from the flooded soil by using 1% ethanol, SiO_2, and argal with the efficiencies of 54.92%, 49.92%, and 41.36%, respectively [24].

For the removal of polyaromatic hydrocarbons (PAHs), copper NPs have been synthesized from plants extracts. Cu-Cs were extracted from *Coriandrum sativum*, and a total of 12 batches of experiments were performed to obtain precise results, and the synthesized NPS were applied as biosorbents. Overall, copper NPs had a removal capacity of 98.07%. In the FTIR analysis, the samples were recorded in the range of 1000–4000 cm at a resolution of 4 cm. Through FTIR results, the best peaks are shown at 470 cm (C O), 424 cm, 413 cm, and 402 cm, respectively. FTIR results indicated that metals have an absorption limit of 300–600 cm which also confirmed the synthesis of NPs [25].

In the same manner, the removal of phosphate is important, and *Sapindus plant* extract was used to synthesize ZrO_2 NO which was used as an absorbent for removal of phosphate. The XDR results showed the average size of NPs as 10.91 nm; FE-SEM results gave the porous and irregular structure of NPs. FTIR and EDX showed a peak at 2,352.2 cm^{-1} which was observed for the first time in the after-adsorption spectrum, and it was estimated to be observed because of the phosphate absorbance with its removal to be in the range of 80.9%-90.3% [26].

Ag-NPs were synthesized from the peel extract of *Citrus maxima* at room temperature. A stable NPs formation was confirmed via SPR (surface plasmon resonance). The presence of silver metal was confirmed by peaks observed at 2.9 and 3.1 KeV via EDS, and a crystalline structure was observed along with face-centric cubic (FCC) lattice in XDR analysis. Ag NPs size ranged from 4 to 11 nm with a spherical shape which was observed via TEM. Naringin, naringenin, and hesperidin were also present with a functional group as O-H along with flavonoid rings was observed under FTIR spectra. Alkaline conditions favor the yield of NPs; hence, a pH of 12 obtained NPs of size 8.6 nm. The ICP-MS revealed the yield of Ag NPs to be about 99%, and the NPs also depicted excellent catalytic activity by degradation of 4-nitrophenol (a pollutant); the NP also had antioxidant properties with anti-bacterial properties too [27].

In another study, Ag NPs were obtained using *Acalypha hispida* extract which acted as a mild reducing agent with stabilizing properties. The dried plant was heated in water, and the extract produced was refrigerated for further use. Ag/MgO nanocomposites were formed, which was confirmed using TEM analysis with an average size of 23 nm and possessing a spherical structure which were immobilized on the MgO surface. This green method has short reaction times with high yields and clean conditions. When $NaBH_4$ was used in water along with Ag/MgO, a high reduction was observed. TEM, XRD, EDS, and FE-SEM techniques were applied to confirm the formation of Ag/MgO. Due to immobilization, the NPs were successfully reused six times [28].

Another set of Ag NPs was synthesized using the *Terminalia bellerica* kernel extract. The NPs showed an average size of 29.6 nm as obtained using TEM. The synthesized silver NPs showed a catalytic reduction of many organic pollutants with a high reduction of 4-nitrophenol than any other organic pollutants. The samples were incubated for 60 min, and a total of 87.0% of 4-nitrophenol was reduced. Kinetic study confirmed that the pseudo-first-order of kinetics was followed. For the NPs, an ANN model was developed and implemented which estimated the catalytic performance of these NPs [29].

The *M. burkeana* plant extracts were taken to synthesize zinc. The sulfisoxazole (SIZ) rate of degradation helped us to evaluate $ZnFe_2O_4$ photolytic activity under UV light irradiation, and a 10-ppm aqueous solution (100 ml) was dispersed. FTIR spectra showed calcination of ZnFe2O4 in 2 h of a time period with a temperature of 700°C. The XDR showed the crystalline structure displaying 2θ diffraction peaks at 53.993°, 62.411°, 35.602°, 53.993°, 49.401°, and 57.560°. The SEM results showed that the NPs had a rod-like structure with a size ranging from 30 to 70 nm. Zn, Fe, and O elements were detected under EDX confirming the formation of NPs. The EPR spectrum detected the para magnetism of the NPs. The optimum pH was 12, and the total removal of sulfisoxazole was 67% in 120 min following the pseudo-second order [30].

Au-Ag NPs were synthesized using *L. inermis* seed extract which had a spherical and irregular shape. To get Au-Ag BNPs, 5 ml of 1 mM $HAuCl_4$ and $AgNO_3$ were taken in a ratio of 1 : 1. The UV-Vis spectra showed a strong SPR center formation at 537 nm which confirms the formation of Au-Ag BNPs. FTIR detected the presence of functional groups (alcohols/phenols, carboxyl, alkaline, and hydroxyl) and aromatic rings. XDR detected the crystalline structure of the NPs with HR-TEM determining the size average size of 32 nm of the NPs, and SAED patterns indicated FCC crystal structure formation in NPs. The donor BH_4 transports its electron to the acceptor 4-nitrophenol, and the entire remediation is dependent on this reduction process. Also, the time taken for reduction was 20 min for 50 ml, 10 min for 100 ml, and 3 min for 150 ml, which indicates that with the decrease in time, the reduction output was also decreased. The entire reaction had its rate constant as 0.5297, 0.2608, and 0.0631 min^{-1} following pseudo-first-order kinetics [31].

A nonsteroidal antiinflammatory drug (NSAID) is a hazardous substance that is being released in water, and some prominently found substances are ibuprofen (Ibu), naproxen (Nap), and diclofenac (Dic), and for the removal of the same green synthesized Cu, nanoabsorbents were used in presence of *Tilia* leaf extract. The XRD results show the diffraction peaks at 2θ ¼ 35, 50.50, and 74.21 with the unit cell having an FCC structure with the UV-Vis analysis of Cu NPs which showed a plasmon peak of at 562 nm. TEM results confirmed well-dispersed spherical and semispherical NPs (4.7 to 17.4 nm). It is understood that the remediation of NSAIDs is entirely pH-dependent with maximum removal efficiency at 4.5 pH. An increase in dosage of Cu NPs increases the removal efficiency, and a similar efficiency increase was seen with the increase in NSAIDs concentrations. The maximum removal of Dic, Ibu, and Nap were found to be 91.4%, 74.4%, and 86.9%, respectively, when set at ideal conditions of 298 K temperature, for 60 min with the dosage of 10 mg Cu NPs under the pH of 4.5 [32].

The *Calotropis gigantea* (CG) flower extracts and dry *Pithecellobium dulce* seed extracts were analyzed for the study. The strong absorption peaks disappeared at the 300 to 350 nm region confirming the polydisperse ZVIN. The bands were seen highest at the range of 3359–3361 cm^{-1} in FTIR analysis which was estimated to be there because of the phenolic groups present for the reduction to Fe^0 from Fe^{+3}. The XRD determined the crystalline structure NPs, and the peaks obtained at 2θ of 45° and 65° in XRD results were because of the Fe_2O_3 presence. The XDR also showed the crystalline structure of the NPs. The SEM analysis showed NPs with a spherical shape within the size range of 50-90 nm. The highest absorbance of alanine was of 74.8% at 12 h time and that of MB was 85.5% in 30 min [33].

The *Mimosa pigra* leaves extracts are used to remove aniline, MB, CR, and hydrogen peroxide (H_2O_2). The characterization of NPs was done using UV-Vis spectroscopy, PXRD, and TEM. 17.5 nm for Ag and 49.5 nm for Ag associated with CuO were the average sizes obtained in the analysis. These plant extracts were used for capping as the O–H and C = O groups. The broadbands appeared in the range of 400–500 nm with some diffractions in the spectrum of Ag-CuO NP. The crystallite size of Ag-CuO at about 50 nm was determined from the XRD results using Scherrer's equation [34].

The *A. elaeagnoidea* flower extracts were used for synthesizing CuNPs, and high levels of phenolic compounds were observed in it, whereas other phytochemicals acted as capping as well as reducing agents. FT-IR band at 450 cm^{-1} which were recognized because of the vibrations of Cu–O gave a confirmation of the NPs formation in addition to proteins and phenolic compounds. XDR analysis showed the crystalline structure with FCC structure. TEM results exhibited the NPs size between 36 and 54 nm, and the NPs showed a high catalytic activity in the aqueous phase for the reducing of MB, CR, and 4-nitrophenol (4-NP) only in presence of $NaBH_4$ at room temperature. Also, by using centrifugation, we can easily recover NPs catalyst and reuse it for up to 6 cycles with still showing a maximum of 90% conversion efficiency [35].

In another study, the research was focused on the green synthesis of magnetite (Fe_3O_4–gINPs) NPs using the coprecipitation method from *Moringa oleifera* and its efficiency for removal of antibiotic; levofloxacin from various aqueous solutions was studied. The average size of the NPs was 14.34 nm and was further evaluated for its adsorption capacity and removal of contaminant. The adsorption batch experiments (adsorbent (NPs) dosage, initial concentration of adsorbate, pH, contact time, and temperature) were conducted to determine the reaction mechanism by studying kinetics while fitting isotherm models. The results exhibited that the maximum adsorption capacity was achieved at equilibrium 22.47 mg/g and that 86.15% removal efficiency of 4 mg l^{-1} levofloxacin was achieved by 100 mg l^{-1} NPs in 24 h contact time. The experiments were conducted in four cycles for reusability and removal efficiency varied from 85.35% to 80.47%, indicating a very high potential of reusability of the adsorbents [36].

The NPs synthesis using plants is an environmentally friendly and inexpensive biological synthesis method. In this study, Ag-NPs were synthesized *via Aloe barbadensis* through biological process which is very environmentally friendly. The FTIR, spectroscopy analysis, and UV-Vis spectrophotometer are used for characterization. The research is based on using silver and copper NPs for wastewater purification. Water contaminated with naphthalene is used in and is further decontaminated and purified using nanoparticles. Similarly, many such other organic compounds are removed with plant-based NPs which are cost efficient, easy, quick, and effective [37].

2.3. Role of Phytonanotechnology for Removal of Dyes. Dye effluents from textile industries have contributed to the worldwide concern of environmental pollution. Various industries exploit over 10,000 distinct forms of dyes and pigments. Diverse forms of artificial dyes are found in wastewaters owing to the poor uptake of those dyes through fabrics. The nature of wastewater can be deciphered when parameters such as oxygen demand (BOD and COD), pH, salinity, temperature, robust color, nonbiodegradable natural compounds, and total dissolved solids present are considered. An integral part of wastewater remediation is green synthesis of NPs and subsequent removal of dyes. Methylene blue, Congo red, malachite green, and methyl green are among the many kinds of dyes retrieved from wastewater resources. NPs of silver, iron, copper oxide, and zinc oxide obtained were analyzed for particle size, and the degradation efficiencies were also calculated [38].

To synthesize NPs using biogenic synthesis, the leaf extracts of *Syzygium cumini* (Jaman) were employed for the degradation of methylene blue. Preceding alcoholic synthesis, the fabrication of ZnO NPs using the leaf extract was calcinated at 500°C for 4 h. The heating was performed at 80°C in the presence of zinc acetate followed by cooling, continuous heating, and filtration. As confirmed by XRD analysis, the ZnO NPs exhibited hexagonal packing and average crystallite size of 11.35 nm. Furthermore, the increase in the pH value resulted in an enhanced degradation (74.3 ± 4.2%, 87.4 ± 2.9%, and 89.96 ± 1.8% at the pH values of 6, 10.4, and 12.6, respectively) of the dye [39].

In addition to phase formation, functionality, and chemical composition, morphological features and surface area of the biohydrothermally synthesized ZnO-$ZnFe_2O_4$ NPs impregnated onto leaf extract of *Psidium guajava*. The prepared NPs (17.8 nm) effectively mediated the water remediation process as well as enhanced the immunity of the plant. At a constant adsorbent dose and contact times between 30 and 180 min, the batch adsorption method served as the ideal means of preparation for the given NPs. When estimated using the pseudo-second order kinetics and Langmuir isotherm models, the maximum adsorption rates were 120.32 mg/g for CR and 90.35 mg/g for MB. Due to high surface-active sites, the dye removal efficiency of CR and MB is at 96% and 90%, respectively [40].

The leaf extract of neem (*Azadirachta indica*) was impregnated with freshly synthesized copper oxide NPs (CuO-NPs) at room temperature. The NPs with an average size of 21.6 nm, synthesized biogenically, degraded 94.5% of total methylene blue dye in 20 min at a higher dose of NPs in 20 ml of 10 ppm dye, under different reaction conditions (time of contact, exposure to UV light, dose, temperature) of the reaction mixture. The recorded dye removal percentage changed from 93.8 to 94.5% at a higher dosage (480 μl) of NPs in 20 ml of 10 ppm [41].

Magnetic ferric oxide NPs (FONPs) were fabricated using the leaf extract of *Peltophorum pterocarpum*. The NPs were 16.99 nm in size and exhibited rod-like and crystalline morphology, showing agglomerations with γ and α-Fe_2O_3 phases after FE-SEM analysis and XRD imaging. With a pore diameter of 7.92 nm, the large FO-NPs were characterized as mesoporous and possessed a surface area of 66.4 m^2/g as per BET analysis. For the MB dye degradation,

the Fenton-like catalytic efficiency of the FO-NPs was estimated at 90% removal within 220 min. A suitable second order model demonstrated the experimental results with a degradation constant of 0.0987 l/mg min. 92% dye degradation within 27 min was obtained when $NaBH_4$ was used as a reducing agent for the evaluation of catalytic potential of the FO-NPs with a first-order model demonstrating the results optimally at a kinetic degradation constant of 0.085/min [42].

Gold NPs (ANL-AuNPs) of size 21.52 nm were impregnated onto plant extracts of *A. nigra* and were characterized by the UV-Vis spectroscopy, FTIR spectroscopy, XRD, and TEM imaging. In the presence of sunlight, ANL-AuNPs catalyzed the degradation of the pollutant dyes, methyl orange, and rhodamine B with percent degradations of 83.25% and 87.64%, respectively. Polyphenolics and other key functional groups present in the aqueous extract played the role of reducing and capping the metal ions in the Au-NPs and were identified using FTIR spectral analysis. Furthermore, this green synthesized NP also exhibited the capacity of inhibiting the growth of some bacteria and antioxidant activity. *Candida albicans*, a pathogenic fungus, were susceptible to this property [43].

The photocatalytic degradation of methyl orange and rhodamine B as anthropogenic pollutant dyes was performed with percent removal of 83.25% and 87.64%, respectively, under a pseudo-first-order kinetic model. The green iron NPs (INPs) were prepared using the *Chlorophytum comosum* aqueous leaf extract. The water dispersion of the leaf extract served as a suitable reducing and capping agent for the spherical, amorphous NPs below 100 nm in size corresponding to their TEM images. Within a span of 6 h, 77% of total methyl orange concentration was eliminated by the synthesized I-NPs. The UV-Vis spectroscopy can reveal the concentration of methyl orange dye by the I-NPs in the presence of H_2O_2. The Antibacterial activity against both Gram-negative and Gram-positive bacteria was suggested by the NPs in addition to dye degradation [44].

Determination of the stability, as well as reusability of the various nanoparticles, was also achieved. The zinc oxide NPs were synthesized in another study in the presence of jujube fruit *Ziziphus jujuba* extract as a reducing agent and a stabilizer. The stable photocatalytic activity was demonstrated by the NPs after sequential degradation experiments. The stability and reusability were determined by stable performance of the NPs up to 4 cycles [45].

The highly efficient and stable photocatalysts were obtained as biogenically synthesized AgNPs using the seaweed extract of *Ulva lactuca.* The Ag-NPs were synthesized biometrically within 48 h of incubation time. The average size of the particles was conformed to be around 48.59 nm and of spherical shape by HR-SEM. The NPs were suggested to be highly stable in colloidal solution due to a negative zeta potential value of −34 mV. At different time intervals, the photocatalytic degradation of the methyl orange dye was investigated using silver nanocatalysts by solar irradiation techniques. Degradation of the dye was visualized by decrease in peak intensity within 12 hours of incubation time [46].

Using plant extract of *Fraxinus chinensis Roxb.* in the presence of the coexisting ions (Pd, Cd), the phytogenic magnetic NPs (PMNPs) were synthesized and functionalized; hence, the material can exhibit high selectivity and faster separation times (35 s). These NPs are suitable for eliminating toxic organic compounds and dyes with visible light illumination under ambient temperature. 3-mercaptopropionic acid (3-MPA) demonstrated an adsorptive capacity of 81.2 mg/g at 25°C and the highest adsorptive rate (98.57% MG removal within 120 min) persisting over a wide pH range (6–12). A removal efficiency of more than 85% was further obtained when the adsorbent (3-MPA@PMNPs) was recovered and reused for a total of five times [47].

Iron oxide and iron NPs are extremely effective NPs for industrial level production. The capping and reducing capacity displayed by the aqueous extract of *Daphne mezereum* was exploited to obtain stable iron oxide NPs (IONPs) ranging from 6.5 to 14.9 nm. The extract prepared after centrifugation resulted in a clear solution that was refrigerated. A mean particle size of 9.2 nm was obtained after preliminary characterization using TEM, particle size analysis (PSA), FTIR spectroscopy, XRD, vibrating sample magnetometer (VSM), and thermogravimetric analysis (TGA). The photocatalytic efficiency of the INPs on methyl orange was investigated and determined at 81% within 6 h using UV-Vis spectroscopy [48].

The iron-silver core-shell nanoparticles, iron-gold core-shell NPs, and iron NPs were synthesized using the pomegranate peel extract (PEP) for the removal of stock solutions of aniline dye from water resources prepared by dissolution of the dye in double distilled water. The FeO/AgNPs less than 100 nm in size showcased iron cores 13 nm in size, while the shell of the NPs was 14 nm in size. Degradation efficiency of the NPs was maximized by optimizing the reaction parameters such as NP and dye concentration, pH, temperature, and contact time, i.e., 30, 60, 90, 120, and 150 min. Substantially higher in alkaline range, the acidic pH proved to be unfavorable for dye removal. 95% and 90% dye degradation efficiency were noted for FeO/Ag-NPs and FeO-NPs at 0.5 mg/ml and 0.25 mg/ml, respectively [49].

High antioxidant content of the peel extract of *Artocarpus heterophyllus* has been reported, and coupled with its bioreducing, capping, and stabilizing potential, it serves as a potential source of valuable biomolecules for the green synthesis of iron NPs (FeNPs) with an average size of 33 nm. Iron oxides and oxyhydroxide form the majority of zero-valent iron NPs (nZVI) and thus obtained. The pseudo-first-order model was used to understand the reaction mechanism at 44.85° C, demonstrating a Fenton-like 87.5% catalytic degradation of pollutant dyes like Fuchsin Basic by the NPs in 20 min [50].

The toxic pollutants such as rhodamine B, BV10 (basic violet 10), BB9 (basic blue 9), AR51 (acid red 51), and BPB (bromophenol Blue) were effectively degraded using green synthesis. The biosynthesized hexagonal wurtzite crystalline zinc oxide NPs (ZnONPs) with nanoflower morphology, zinc, and oxygen bonding vibrations at 557 cm^{-1}, 511 cm^{-1}, and 433 cm^{-1} (FTIR) and an average size of 13.33 nm were characterized by the UV-Vis spectroscopy, SEM, EDS, XRD, BET, and other techniques to contain phytocomponents retrieved from the zinc acetate precursor and leaf

extract of *Cyanometra ramiflora* that can aid in the reduction of zinc ions. At 360 nm in the UV-Vis curve, a sharp absorption maximum was observed, indicating that the formation of ZnO NPs strong signals were exhibited by EDS for zinc and oxygen elements. 98% photocatalytic removal within 200 min of contact under sunlight irradiation against rhodamine B with a degradation constant of 0.017 min^{-1} suggested a remarkable degradation efficiency [51].

The dried flowers of *Convolvulus fruticosus* were macerated, filtered, and condensed to obtain a pure solid flower extract for the synthesis of gold NPs with an average particle size of 35 nm after the FE-SEM, TEM, and DLS analysis. The degradation of the dyes were accounted to be 94.3%, 90.2%, and 85.4% under UV and 80.6%, 79.8%, and 73.3% under visible light irradiation for basic violet 10 (BV10), basic blue 9 (BB9), and acid red 51 (AR51), respectively, demonstrating the photocatalytic capacity of the NPs [52].

Filtered extract of the seed powder obtained from *Punica granatum* seed extract was used after centrifugation for the fabrication of irregular-shaped hematite nanoparticles. The synthesized α-Fe_2O_3 NPs exhibited an average size of 26.53 nm as indicated by the FE-SEM and TEM analysis. The BET analysis on the other hand revealed a stable yet sustainable nature of the NPs, with a surface area of 31.52 m^2/g, and an average pore diameter of 5.54 nm was calculated. The variations in the initial concentration of the dye and temperature correspond to a bell curve when correlated to dye degradation efficiency. The experimental results followed the pseudo-first-order kinetics and reported a remarkable 89.42% solar light-driven photocatalytic degradation potential of anionic Congo red and 87.96% for bromophenol blue in 240 min at ambient conditions [53].

2.4. Role of Phytonanotechnology for Removal of Pathogens. Global public health is now facing an alarming threat in the form of human pathogens. Resembling the intestines of an individual, the wastewater treatment plants (WWTPs) serve an important role of receiving and digesting various pathogens infringing on human lives. Phytonanotechnology is one such strategy that enables the removal of pathogens from WWTPs in an eco-friendly, affordable, and effective manner.

The biocidal properties of copper and copper-associated complexes coupled with their relative ease of availability in plant biomaterials, exceptional thermal, and electrical conductivity make them ideal bioabsorbents and antimicrobial agents. CuO NPs were incorporated into the plant extract of *Madhuca longifolia*, which is a nontoxic reducing agent and has high biocompatibility. XRD patterns revealed peaks at $2\theta = 32.58^\circ$, 35.15°, 35.67°, 36.64°, 38.86°, 49.05°, 57.51°, and 58.46°, while FTIR spectra affirm crests for Cu–O bonding at 480, 540, 660, and 670 cm^{-1}. The UV-Vis spectroscopy studies revealed mixed phase Cu $(OH)_2$ and CuO NPs being formed in the process with peaks within the range of 240–390 nm. Furthermore, distinctive spikes around 380 and 480 nm values determine the formation of NPs as valid. TEM suggested that the NPs have a spherical structure with the size of 120 nm which were dispersed evenly, but at some points, aggregations of the same were also observed. Using the well diffusion method, the bacterial removal capacity of the composites was checked for *E. coli BL21 DE3*, *S. aureus*, and *B. subtilis*, which largely depends on the size of the nanoparticles, their concentration, and stability along with the concentration of the growth medium and the type of bacterial cultures tested against the nanoparticles. Zones of inhibition in the range of 15.67 ± 058 mm and 14.67 ± 058 mm suggest moderate removal efficiency against *S. aureus*, *B. subtilis*, and *E. coli BL21 DE3*. Lastly, photocatalytic removal of MB under visible light irradiation is affected by agglomeration and is capped at 77% and 46% for the two samples [54].

The innovation of a novel, green, economical, and reproducible chemical reduction method that employs shredded bagasse and rice husk subsuming copper NPs (for the potential treatment of potable water *via* the removal of *E. coli*) was carried out by Bashir et al. The inductively coupled plasma optical emission spectroscopy (ICP-OES) analysis captured an increment in copper concentration in modified rice husk and bagasse as up to 38.5 mg/g and 29.9 mg/g as compared to 2.7 mg/g and 3.6 mg/g in their respective raw forms. The SEM analysis highlighted the absence of any ligand or stabilizing agent as a supplement, which resulted in undulating surfaces on fiber bundles and aggregation of Cu-NPs. When used in the range of 0.5–3.0 g/100 ml of water at a pH between 5 and 9 and a contact time of 100–120 min, the antimicrobial removal efficiency increased nearly twofold from 46% to 95% for bagasse and 48% to 100% for rice husk incorporated with nanoparticles, lasting for a period of 5 weeks [55].

Silver and silver-related compounds are highly sought-after in commercial markets due to their desirable chemical stability, catalytic, and antimicrobial activity alongside copper. The *Phyllanthus pinnatus* stem extract was used for the biogenic fabrication of silver NPs (AgNPs) less than 100 nm in size (SEM). Alkaloids, saponins, alcohols, phenols, terpenes, and proteins accelerate the synthesis of these NPs and reduce Ag^+ to Ag with minimal cost, less time, and absence of any toxic by-products. λ_{max} absorption peak was obtained at 490 nm by SPR from the UV-Vis spectroscopy, while the peaks at 3316 cm^{-1}, 1603 cm^{-1}, and 1036 cm^{-1} highlight the stretching of O–H, bending of C = C, and vibration of C–N from FTIR. C–H stretching at 2918 cm^{-1} possibly indicates the presence of methylene groups within the proteins, while O–H stretching could be linked to the bioreduction of the AgNPs by hydroxyl groups. The morphology of the NPs was described as crystalline by XRD studies and cubical, triangular, or spherical in shape at different magnifications according to SEM images. The antimicrobial activity was assessed *via* Kirby-Bauer disc diffusion assay on *V. cholera*, *S. flexneri*, *P. aeruginosa*, *M. smegmatis*, *P. vulgaris*, and *B. subtilis*. The NPs exhibited dose-dependent inhibition with maxima at 1.8 mm (40 μl) for both *V. cholera* and *S. flexneri* and 1.5 mm at 10 μl for *V. cholera* suggesting its sensitivity to the nanocomposite [56].

The biosynthesis of AgNPs was optimized by the UV-Vis method and facilitated with corn cob extract obtained from *Zea mays* in another study. The corn cob (CC) extract is rich in phenols, glucosides, and anthocyanins that offer

the property of antioxidation, while high contents of hemicellulosic sugars are useful for the fabrication of CC-AgNPs as agents for reduction or capping. UV-Vis analysis confirmed metallic NP formation through SPR bands formed between 400 and 430 nm. FTIR spectra have elicited strong bands at 3285 cm^{-1} for hydroxyl groups which shifted to 3334 cm^{-1} upon reduction with Ag. Furthermore, aryl ketones containing C = O bonds stretch at 1626 cm^{-1}, while the extract itself shows peaks for phenolic and aromatic groups at 1350 cm^{-1} and 1412 cm^{-1}. The powder XRD patterns provoke characteristic peaks at 2θ values 38.2°, 43.2°, 63.8°, and 77.0°, and through Scherrer's equation, the resulting average crystallite size is estimated to be 13.55 nm for CC-AgNPs, while TEM studies show that the NPs are sized between 2 and 28 nm with spherical morphology. The antibacterial assays were performed using the diffusion method in the range of 0.5–8.0 μg/ml. CC-AgNPs exhibited dose-dependent inhibition with remarkable results at 8.0 μg/ml against *B. cereus* and *S. aureus* but not so much for *S. typhimurium*. Auxiliary investigations into the potential of the nanocomposite to behave as photocatalysts for the degradation of o-, m-, and p-nitrophenols and dyes such as Eosin Y and rhodamine 6G were also conducted with promising findings [57].

Malini, Kumar, and Hariharan et al. demonstrated the synthesis of chitosan-encapsulated green synthesized silver NPs (AgNPs) utilizing leaf extract of *Prosopis juliflora* using a simple ionic gelation method. The UV-Vis spectroscopy indicated absorption maxima at a wavelength of 420 nm, and distinctive peaks at 440 nm due to surface plasmon resonance of the oscillating electron present in the conduction band signify their biosynthesis. SEM imaging supported the findings from the UV-Vis spectroscopy, showing and smooth-surfaced nanocapsules with spherical morphology with average dimension of a particle as 30 nm as per the Debye-Scherrer equation. FTIR spectra of the plant extract confirmed its dual role as a reducing and capping agent due to the identification of key functional groups such as phenols (3409.28 cm^{-1}), alcohols (2929.28 cm^{-1}), alkanes (1774.43 cm^{-1}), ketones (1631.70 cm^{-1}), and aromatic compounds (1047.79 cm^{-1}). Leads were also obtained on the possibility of interaction between the AgNPs and NH_2 groups present in chitosan. Zone of inhibition measuring 22 mm was obtained during antibacterial assays of *E. coli* test cultures against a culture of streptomycin as the positive control. Additionally, their capacity of removing heavy metals *via* bioadsorption and 83% photocatalytic degradation of rose Bengal dye within 2 h of contact provides us with a promising agent for the removal of water contaminants [58].

Asparagus racemosus was used to prepare silver NPs *via* a greener, eco-benign, and facile route. XRD pattern analysis catalogued the FCC structure of metallic silver, as well as the average crystallite size of the NPs to be around 20 nm. FTIR spectra demonstrated the presence of phenols, carboxylic acids, and amide linkages commonly noted in proteins. The scanning electron microscopy-energy dispersive X-ray analysis (SEM-EDX) investigation certified the formation of silver NPs as well as the presence of minute, spherical NPs, while the larger ones were formed possibly due to aggregation of smaller NPs. TEM images estimated the average size of NPs between 17 and 25 nm with smaller NPs reaching just beneath 10 nm. The antibacterial activity of the nanocomposites was assayed using Agar well diffusion; the NPs were dissolved in DMSO, and the wells were loaded with 50 μl (100 μg/ml) of AgNPs and incubated with cell cultures for 24 h. The MIC value for *P. fluorescence*, *Y. ruckeri*, *E. tarda*, and *E. coli* stood at 25 μg/ml and 12.5 μg/ml for *A. hydrophila*, *F. branchiophilum*, *K. pneumoniae*, *S. aureus*, and *B. subtilis*. The inhibition zones formed by AgNPs were 17.0 ± 0.89 mm and 16.0 ± 0 mm for *S. aureus* and *B. subtilis,* respectively, followed by 15.66 ± 0.51 mm, 14.5 ± 0.54 mm, 14.5 ± 0.54 mm, 13.16 ± 0.75 mm, 13.16 ± 0.75 mm, 13.0 ± 0.89 mm, and 12.33 ± 0.51 mm for *F. branchiophilum*, *A. hydrophila*, *K. pneumoniae*, *E. tarda*, *Y. ruckeri*, *P. fluorescence*, and *E. coli*, respectively. The enhanced antimicrobial activity of the nanocomposites and protection against aggregation was attributed to the metabolites present in root [59].

A facile, eco-friendly, and nontoxic chemical method was used to synthesize silver NPs (AgNPs) and incorporated onto the leaf extract of *Pergularia daemia*. The biogenic synthesis of the composite can be confirmed by a preliminary examination with $AgNO_3$, UV-Vis spectrophotometry, and checking for SPR band peaks at 420 nm. The face-centered cubic (FCC) structure of fabricated NPs was affirmed by XRD patterns which elicited diffraction peaks at $2\theta = 37.4°$, 46.1°, 64.2°, 78.1°, and 85.2°. FTIR peaks at 3415.31 cm^{-1} and 1600.63 cm^{-1} indicate the presence of functional groups like carboxylic acids and aliphatic or aromatic amines, respectively, that assist in the formation of AgNPs. FE-SEM analysis revealed that the silver NPs are spherical, do not aggregate, and show a size distribution of 30–45 nm. The dose-dependent antibacterial activity was measured against *E. coli* using well diffusion where varying concentrations of AgNPs were chosen as 10, 30, 70, and 90 μl. Lower concentrations (10 and 30 μl) demonstrated moderate inhibition and inconspicuous zones of inhibition, while higher concentrations (70 and 90 μl) produced clear inhibition zones. AgNPs showed significant antibacterial activity against most Gram-negative bacterial pathogens which suggests that the NPs can be used as an excellent biocidal agent [60].

Paradigm altering microwave and ultrasonically modified methods were combined and used in addition to *Citrus paradisi* peel extracts to synthesize a multifunctional, 3-layered Ag-MgO/nanohydroxyapatite (Ag-MgOnHaP) nanomodel. The UV-Vis analysis alludes to the color variation from light yellow to dark brown as well as the achievement of absorption maximum at 440 nm, which affirm the fabrication of silver nanoparticles. Formation of two intense bands at 290 nm and 378 nm denote the coalition of MgO with AgNPs and a blue shift of AgNPs from 440 nm to 378 nm, respectively. SEM images disclosed irregular flake-like morphology but soon transitioned to highly fine discrete shapes upon exposure to ultrasound. An Ag-MgOnHaP composite when subjected to TEM and ultrasound exposure between 20 and 100 nm resulted in an average mean particle size of 16.44 nm. The antimicrobial

capacity of the nanocomposite for *E. coli* subsequently formed 13 mm wide zones of inhibition, and 10 mm for *K. pneumoniae*. The defluoridation capacity through adsorption for these composites is 90% at 0.3 g dosage, 2.146 mg/g at 298 K. The sorption process follows the second order kinetics at room temperature and fit in well with Freundlich isotherms [61].

In another report, Naghizadeh et al. implemented a green, rapid, feasible, and cost-effective method for the synthesis of silver NPs (AgNPs) using *Jujube* core extract. The nanocomposites were prepared using a simple biogenic chemical method based on physicochemical characteristic studies to the likes of surface plasmon resonance (SPR) where peaks were obtained at about 420 nm. HPLC assay using a UV-Vis spectrophotometric detector at 275 nm attributed the biological activity of the extract to the presence of epicatechin, gallic acid, caffeic acid, p-coumaric acid, ferulic acid, and rutin. The crystalline structure of the NPs was ascertained using XRD patterns with sharp peaks at $2\theta = 38.09^\circ$, 44.3°, 64.52°, and 77.43°. Images from FESEM and TEM estimated the average particle size between 25 and 50 nm, and 34 nm using Scherrer's equation. Furthermore, declining intensity in SPR bands confirmed their optimal interaction period at 30–45 min. MIC and MBC values (μg/ml) were the least for *E. coli* at 1.25 and 1.25, which comments on their enhanced sensitivity, while *K. pneumoniae* and *S. aureus* are comparatively more durable against the nanocomposites with MIC and MBC values of 2.5 and 2.5 and 2.5 and 10, respectively. These findings were supported by the large surface area-to-volume ratio of AgNPs which helps in establishing contact. Lastly, anticancer and photocatalytic activities of the NPs against AGS cell line and eriochrome black T and rhodamine B were also demonstrated under UV and visible light irradiations [62].

Self-propagating sol-gel autocombustion was used for green, facile, economical, and eco-benign synthesis of silver doped copper and zinc nanometal oxides impregnated onto *Sida rhombifolia* leaf extract. Diffraction peaks obtained through XRD analysis estimates the average crystalline size of Ag/CuO NPs at 2.18 nm. FESEM reports show that Ag/CuO are rod-shaped nanostructures while other variants of the NP may show spherical or quasispherical morphology. Antibacterial assays were conducted using agar diffusion, and the inhibition potential of Ag/CuO NPs was the highest within the group. The MIC zone for *E. coli* (10 mm), *K. pneumoniae* (19 mm), *S. aureus* (13 mm), and *S. mutans* (8 mm) was 1 mg, while it was 3 mg for *P. aeruginosa* (8 mm). Thus, we can assume that Ag-doped CuO NPs are the most hostile species of nanohybrids against pervasive pathogens. Uses of Ag/CuO nanorods is also elicited in photocatalytic removal of methyl green (MG) and methylene blue (MB) with 90% efficiency as well as the removal of 4-nitrophenol [63].

Metallic NPs can also be synthesized using metals such as zinc, iron, titanium, or their complexes. In one paper, ZnO NPs were synthesized from zinc acetate dihydrate and impregnated with fruit peel extract obtained from orange. The bioreductive and capping capacity of the biomaterial prohibit growth of undesired pathogens such as *E. coli* and *S. aureus* from water. TEM images suggest that the NPs are relatively small and spherical (between 10 and 20 nm) and aggregate in large clusters within the organic material earlier present in the reductant. XRD patterns assert 12 nm as the smallest average crystalline size which can increase for higher annealing temperatures. The presence of phenols, alcohols, alkanes, ketones, and aromatic compounds was confirmed in FTIR in the wavenumber range of 3409.28 cm^{-1}, 2929.28 cm^{-1}, 1774.43 cm^{-1}, 1631.70 cm^{-1}, and 1047.79 cm^{-1}. The FTIR spectra also elicit bands of alkene and carbonyl groups on the surface of the NPs. The antimicrobial property of orange-peel extract is maintained by aromatic and saturated organic molecules such as tannins, saponins, phenolic compounds, flavonoids, and essential oils as reactive oxygen species (ROS). Thus, ZnONPs showed exceptional performance in inhibiting the growth of *E. coli* at 0.025 mg/ml after 8 h of incubation, with bactericidal rates of 99.96% to 99.99% and 94.29% for *S. aureus* [64].

$ZnFe_2O_4$/reduced graphene oxide nanohybrids (G-$ZnFe_2O_4$/rGO NHs) with high specific surface area, favorable electron transportation, good thermal and electrical conductivity, and biocompatibility that serve as an effective measure to control bacterial growth were synthesized using a natural surface-active peel extract. XRD patterns highlighted the successful formation of $ZnFe_2O_4$ with rGO as the G-rGO phase can be seen at $2\theta = 26.35^\circ$. The results from FTIR proved the presence of different essential oxygen-containing functional groups such as carbonyls, hydroxyls, and ethers at 1632 cm^{-1}, 1401 cm^{-1}, and 1198 cm^{-1}, respectively. HR-TEM and SEM imaging allow us to observe the regular, smooth surface morphology of the NPs on rGO sheets with an average size of 30 nm. Photobacterial experimentation on G-$ZnFe_2O_4$ and G-$ZnFe_2O_4$/rGO NHs demonstrated significant results as the bacterial removal was reduced to $70.57 \pm 4.2\%$ upon being exposed to visible light for 40 min due to the synergistic action of ROS generation. Similarly, the nanohybrids also displayed tremendous cytotoxic activity against A549 cell line with an IC_{50} value of 249.9 μg/ml and, thus, can be used to removal organic dyes or pathogens from water [65].

Zingiber officinale (ginger) extracts were explored as an antimicrobial agent in conjunction with iron NPs (FeNPs) using a green, eco-friendly, facile, and benign approach as it offers anticancer, anticlotting, antidiabetic, antiinflammatory, and antioxidant effects. UV-Vis spectroscopy elicited characteristic peaks at 406 nm, while FTIR spectra when recorded between 500 cm^{-1} and 4000 cm^{-1} corresponded with the stretching of OH, C–H, and Fe–O bonds. XRD analysis implied that the synthesized NPs were 5.10 nm in size with $2\theta = 32.43^\circ$ and exhibited magnetite phase. SEM imaging showed stable nanocube-like crystalline structures. The nanocomposites expressed good antibacterial activity at 80 μl and 100 μl concentrations with zones of inhibition of *E. coli* at 20 and 22 mm when incubated for 24 h, respectively, as compared to the extract independently. Thus, this approach can be considered as a reliable and conclusive method for treatment of pathogens from water [66].

Pod extract from *Peltophorum pterocarpum* contains polyphenolic compounds, non-protein amino acids, polysaccharides, bergenin, and other metabolites that supplement the

Table 1: Summary of the application of plant source-mediated nanoparticles in the remediation of wastewater contaminants.

No.	Biomaterial	Name of biomaterial	Nanoparticles	Size of NPs	Contaminant removal	Capacity of removal	Time taken	Miscellaneous	Ref.
1.	Leaf extract	*Ziziphus jujuba*	ZnO	20 nm	Pb(II)	80.68%	30 min	The maximum removal of the Pb(II) was obtained by the application of the MWG ZnO NPs, compared with the G ZnO NPs, MWT ZnO NPs, and T ZnO NPs	[18]
2.	Leaf extract	*Syzygium Cumini*		10-12.55 nm	Methylene blue dye	91.4%	180 min	Photocatalytic degradation activity	[41]
3.	Fruit extract	*Ziziphus jujuba*		20-37 nm	Methylene blue (MB) Eriochrome black T (ECBT)	Degradation efficiency 85% TOC removal 65%	5 h	Has potential for the treatment of industrial wastewater from textile and rubber industries	[45]
4.	Leaf extract	*Cyanometra ramiflora*		13.33 nm	Rhodamine B dye	98%	3 h 20 min.	Antimicrobial activity, used in medicine, textiles, and cosmetics	[51]
5.	Leaf extract	*Sida rhombifolia*		3.42 nm	*Escherichia coli, Klebsiella pneumoniae*, *Pseudomonas aeruginosa*, *Streptococcus mutans*, and *Staphylococcus aureus*		24 h	Antibacterial studies indicated that the NPs have the ability to destroy both Gram-positive and Gram-negative bacteria	[63]
6.	Peel extract	*Orange*	$ZnFe_2O_4$	30 nm	*Escherichia coli*	70.57% ± 4.2%	40 min	Due to the synergistic action of ROS generation, the nanoparticles exhibited excellent antibacterial properties	[65]
7.	Plant extract	*M. burkeana*		25.03 nm	Methylene blue and sulfisoxazole	99.8%	45 min	Zinc ferrite nanoparticles Photocatalytic effect and degradation	[30]
8.	Leaf extract	*Psidium guajava*	ZnO–$ZnFe_2O_4$	17.8 nm	Congo red and methylene blue	96% of CR and 90% MB	150 min	The fabricated ZnO–ZnFe2O4 NPs enhance the plant immune response and promote plant growth, potentially by preventing transpirational water loss	[40]
9.	Bagasse and rice husk	Sugar and rice plant	CuNPs		*E. coli*	Up to 100%		Bacterial removal efficiency of CuNPs incorporated rice husk was measured 100%, higher than 95% achieved by using CuNPs incorporated bagasse	[55]
10.	Leaf extract	*Azadirachta indica*			Naphthalene	98.07%	0-30 min	Bioabsorbent for decontamination of PAH	[69]
11.	Leaf extract	*Tilia* leaves		0.34–1.27 nm	Ibuprofen (Ibu), naproxen (Nap), and diclofenac (Dic)	Ibu: 74.4% Nap: 86.9% Dic: 91.4%	60 min	Follows the second order kinetic model for sorption; adsorption process was spontaneous and endothermic	[32]
12.	Plant extract	*Madhuca longifolia*	CuO	30-120 nm	*E. coli* BL21 DE3 Gram-negative, *S. aureus* Gram-positive, and *B. subtilis* Gram-positive		24 h	Selectively effective against various strains of microorganisms	[54]

Table 1: Continued.

No.	Biomaterial	Name of biomaterial	Nanoparticles	Size of NPs	Contaminant removal	Capacity of removal	Time taken	Miscellaneous	Ref.
13.	Leaf extract	*Azadirachta indica*		21.6 nm	Methylene blue	93.4-93.75% (lower dose) 93.8-94.5% (higher dose)	0-20 min	The leaves extract contains phytochemicals which act as reducing, capping and reducing agents	[41]
14.	Flower extract	*Aglaia elaeagnoidea*	Copper nitrate	20–45 nm	4-Nitrophenol	90%	—	Catalytic activity on pernicious dyes such as Congo red and methylene blue; NPs can be recovered and reused for 6 cycles by centrifugation	[35]
15.	Stem extract	*Phyllanthus pinnatus*		>100 nm	*V. cholera*, *S. flexneri*, *P. aeruginosa*, *M. smegmatis*, *P. vulgaris*, *B. subtilis*		24 h	Zones of inhibition formed shows efficient antibacterial activity	[56]
16.	Root extract	*Asparagus racemosus*		10-17 nm	*Escherichia coli*, *Staphylococcus aureus*, *Bacillus subtilis*, *Klebsiella pneumonia*, *Pseudomonas fluorescens*, *Aeromonas hydrophila*, *Edwardsiella tarda*, *Flavobacterium branchiophilum*, and *Yersinia rukeri*		24 h	Economical eco-friendly and green synthetic material	[59]
17.	Leaf extract	*Prosopis juliflora*		30 nm	*Escherichia coli*, Rose Bengal dye, heavy metal	83% - rose Bengal dye 81% - heavy metals	24 h, 0-30 min, 45-180 min, respectively	Nanoparticles synthesized can be used for wastewater treatment	[58]
18.	Leaf extract	*Pergularia daemia*		30-45 nm	*Escherichia coli*		24 h	AgNPs can be used as a good biocidal agent against bacterial pathogens	[60]
19.	Leaf extract	*Aloe barbadensis Azadirachta indica Coriandrum sativum*	AgNPs		Naphthalene decontamination	90%		Three different plants precursors are used for the synthesis of plant extracts such as *Aloe barbadensis*, *Azadirachta indica*, and *Coriandrum sativum* that are further used to synthesize nanoparticles. Two different nanoparticles are obtained such as silver nanoparticles (Ag-NPs) and copper nanoparticles (Cu-NPs)	[69]
20.	Kernel extract	*Terminalia bellerica*		32 nm	4-Nitrophenol	87%	60 min	ANN modeling was used as it does not require mathematical description of the phenomena involved in reduction process	[29]
21.	Leaf extract	*Mimosa pigra*		17.5 nm	Methylene blue, hydrogen peroxide	55-60% MB 22-45% H_2O_2	48 h	Displayed excellent photocatalytic properties	[34]
22.	Peel extract	*Citrus maxima*		4 – 11 nm	4-Nitrophenol	~100%	50 min	Excellent antioxidant and antimicrobial action against *E. coli*, *F. oxysporum*, and *V. dahliae*	[27]

Table 1: Continued.

No.	Biomaterial	Name of biomaterial	Nanoparticles	Size of NPs	Contaminant removal	Capacity of removal	Time taken	Miscellaneous	Ref.
23.	Husk extract	*Juglans*		46.2 nm	Petroleum wastewater (Pb, Cr, Cd)	Pb 72.6% Cr 81.3% Cd 88.1%	5 h	New nanoscale bio-based nanocomposite	[13]
24.	Leaf extract	*Piliostigma thonningii*		70-114 nm	Cu^{++}	82.1%	1 h	Treatment of diseases such as ulcers, diarrhea, dysentery, worms, and other intestinal problems	[19]
25.	Leaf extract	*Ficus benjamina*		60-105 nm	Cd^{++}	75.5% (100 mg/L) 85% (50 mg/L)	40 min	In a source of indoor allergens, symptoms include allergic asthma and rhino-conjunctivitis	[14]
26.	Seed extract	*Moringa oleifera*		9.4 nm	Pb^{++}	>80%	30 min	Photocatalysis of organic dyes and compounds and antimicrobial activity	[70]
27.	Peel extract	*Citrus paradisi*	Ag-MgO	16.44 nm	*Klebsiella pneumonia* and *Escherichia coli*		24 h	Ag-MgO served a dual purpose both in defluoridation and antimicrobial activity	[61]
28.	Plant extract	*Acalypha hispida*		23 nm	Methylene blue, methyl orange, 4-NP, 2,4-DNPH		60 s -120 min	Effective in the reduction of pollutants using NaBH4 in water	[28]
29.	Fruit extract	*Jujube*	AgNPs-JCE	25–35 nm	*E. coli* and *K. pneumoniae* as Gram-negative bacteria and *S. aureus* as Gram-positive bacteria		Up to 45 min	FESEM, TEM, XRD, FT-IR, EDS, and UV–Visible spectroscopy	[62]
30.	Ginger extract	*Z. officinale*		5.10 nm	*E. coli*		24 h	*Zingiber officinale* root has important role in pharmaceutical industry	[66]
31.	Leaf extract	*Chlorophytum comosum*	FeNPs	<100 nm	Methyl orange dye	77%	6 h	(Iron nanoparticles) INPs are also employed as a Fenton-like reagent	[44]
32.	Peel extract	*Artocarpus heterophyllus p*		33 nm	Fuchsin basic dye	87.5%	20 min	The peel has high antioxidant content which is a valuable biomolecules and act as the bioreductants	[50]
33.	Leaf extract	*Daphne merezeum*	Fe_2O_3	9.2 nm	Methyl orange dye	81%	6 h	Daphnin and mezerein are two toxins produced by the plant. It is also used as an ornamental plant	[48]
34.	Leaf extract	*Peltophorum pterocarpum*		16.99 nm	Methylene blue dye	90%	3 h 40 min	In an ornamental tree, its foliage is used as a fodder crop	[42]
35.	Seed extract	*Punica granatum*	α-Fe_2O_3	5.54 nm	Congo red (CR) and bromophenol blue (BPB)	89.42% for CR and 87.96% for BPB dye	240 min	The magnetic properties of the material are directly related to their recovery and reuse in practical applications	[53]
36.	Leaf extract	*Moringa oleifera*	Fe_3O_4	14.34 nm	Levofloxacin	86.15%	24 h	The potential pathway for the removal was by chemisorption	[37]

Table 1: Continued.

No.	Biomaterial	Name of biomaterial	Nanoparticles	Size of NPs	Contaminant removal	Capacity of removal	Time taken	Miscellaneous	Ref.
37.	Peel extract	*Punica granatum*	FeO/Ag	27 nm	Aniline blue (AB) dye	11-90%	30-150 min	Suitable for application in water purification techniques	[49]
38.	Leaf extract	*Simarouba glauca*	GT-nFe	9 nm	Lead (II)	80%	5-60 min	The obtained NPs were reused for up to 3 times	
39.	Leaf extract	Green tea			Cr(VI)	99.9	60 min		[10]
40.	Leaf extract	Barberry plant	GnZVI	20-40 nm	Cr(VI)	100%	5 min	Experiments were performed in a batch photoreceptor	[8]
41.	Black tea (BT)	Powder extract	ZVI NPs	6.1 to 10.6 nm	Cu2+	82%	50 min	By using the effect of gamma radiation at ph, the removal of Cu2+ metal ions increased up to 97%	[17]
42.	Flower extract	*Calotropis gigantea*		30 nm	Aniline	49.4%	12 h	Decolorization of toxic textile dyes like methylene blue	[33]
43.	Leaf extracts	*Ipomoea carnea Ficus sycomorus*	Ag and F–Fe0	F–Fe0: 2.46 nm to 11.49 nm Ag: 6.27 to 21.23 nm	Chlorfenapyr	Variable	1-2 weeks	Iron nanoparticles (F–Fe0) and Ag with different absorbants have different efficiencies and time requirement	[24]
44.	Fruit extract	Lemon		22-54 nm	Pb	100%		The synthesized NPs were of varied shapes	
45.	Flower extract	*Convolvulus fruticosus*	AuNPs	35 nm	Basic violet 10 (BV10) Basic blue 9 (BB9) Acid red 51 (AR51)	73.3%-94.3%	15-60 min	Essential for biological and removal of toxic pollutants for water purification	[52]
46.	Leaf extract	*Alpinia nigra*		21.52 nm	Methyl orange dye	83.25%	2 h	Antioxidant and antimicrobial activity	[43]
47.	Seed extract	*Lawsonia inermis*	Au-Ag	15-35 nm	4-Nitrophenol	100%	3-20 min	A simpler and greener method for the synthesis of Au-Ag NPs using the aqueous fraction of *L. inermis* seed extract with ultrasonification	[31]
48.	Leaf extract	Eucalyptus			Triclosan (TCS) and copper (Cu(II))		9 min	The residual concentrations of TCS were determined using an Agilent Technologies 1260 Infinity II HPLC system equipped with a UV detector	[23]
49.	Straw waste		Bimetallic Fe/Ni NPs		Cr(VI)	58.1% to 99.7%	4 h	XRD, SEM, XPS, and nitrogen sorption isotherms were employed to completely characterize the obtained FeNi@HPC	[11]
50.	Leaf extract	Green tea	rGO-Fe/Ni	20–80 nm	Sb(III)	95.7%	3 h	Bimetallic iron/nickel nanoparticles were loaded with graphene oxide forming rGO-Fe/Ni	[15]

Table 1: Continued.

No.	Biomaterial	Name of biomaterial	Nanoparticles	Size of NPs	Contaminant removal	Capacity of removal	Time taken	Miscellaneous	Ref.
51.	Rice residue		ZBC		As(III) and As(V)	—	Variable	Zirconium (hydro) oxide (Zr(OH)4 or ZrO2) particles have been documented as a potential adsorbent agent for the removal of As(III) and As(V) from waters	[16]
52.	Peel extract	*Pomegranate*	TiO_2	92.8 nm	*Staphylococcus aureus*, *Escherichia coli*, *Pseudomonas aeruginosa*	99.9%	24 h	PPP-TiO_2 was confirmed to have antibacterial susceptibility properties against Gram-positive and Gram-negative bacteria	[68]
53.	Plant extract	*Konjac glucomannan*	Pd NPs	6.48 ± 2.19 nm	Cr(VI)	—	—	Calculated absorbance were 93.4% by 120 min, 89.1% by 90 min, 83.2% by 135 min, 79.3% by 150 min, 77.1% by 120 min, and 70.1% by 250 min for MO, AR I, PC, AV7, GO II, and AO74 degradation, respectively	[9]
54.	Leaf extract	*Fraxinus chinensis Roxb.*	Phytogenic magnetic nanoparticles (PMNPs)		Malachite green (MG)	98.57%	2 h	The equilibrium adsorption time was different for the different concentrations of MG dye	[47]

formation of magnetite (Fe_3O_4) NPs. Visual studies show that the solution changes color from colorless to greenish black. UV-Vis experiments do not yield a distinct peak but more so a continuous absorption band spanning from 300 nm to 800 nm. SEM analysis confirmed the spherical morphology of NPs with little to no aggregation. EDS was crucial in uncovering the primary elements present in the composite (Fe and O). Powder XRD pattern of PP-Fe_3O_4 NPs revealed several sharp peaks which helped in determining the crystallite size of the NPs as 23.82 nm. Bactericidal action of the PP-Fe_3O_4 NPs is enhanced because of their high surface area-to-volume ratio. Using agar well-diffusion assay on *E. coli* and *S. epidermidis*, the zones of inhibition were noted at 15 and 12 mm, respectively; for 60% concentration, 18 and 13 mm, respectively, for 80% concentration; 19 and 15 mm, respectively; and for 90% concentration, and 20 and 16 mm, respectively, at 100% concentration when incubated for 24 h with PP-Fe_3O_4 NPs. Lower values of inhibition zone for *S. epidermidis* stems from its thick peptidoglycan layer which can resist the penetration of the PP-Fe_3O_4 NPs. Similarly, the photocatalytic potential of the PP-Fe_3O_4 NPs was calculated to be 88.98% for MB dye 45 min after exposure [67].

Pristine pomegranate peel extract (PPP) was impregnated with TiO_2 NPs to fabricate metal matrix nanocomposites (MMC) capable of inhibiting microbial growth for the treatment of water resources. Characterization of the NPs began with SEM imaging where the images of PPP before and after loading with TiO_2 NPs were visualized. Arbitrarily oriented and irregular grains with sharp boundaries, microcracks, and aggregates could be seen. On the other hand, large grains with smooth surfaces, sharp boundaries, and no discernible eruptions were observed in PPP- TiO_2 NPs. Surface charge present on the NPs was evaluated using ζ-potential values. For TiO_2 NPs, ζ-potential is -6.95 mV and is -11.4 mV for PPP-TiO_2 NPs signifying a good distribution of particles. Powder XRD patterns estimate average crystallite size of TiO_2 NPs is 92.8 nm using Scherrer's equation. The XRD pattern of PPP exhibited single broad peak signifying amorphous character, and thus, calculating the average crystallite size can be difficult. The broth microdilution method was used for the assay where MIC_{50}, MIC_{90}, and MBC for each of the three microorganisms were estimated. 99.99% of *S. aureus* colonies were eliminated at 200 μg/ml, and the same removal efficiency for *E. coli* and *P. aeruginosa* could be achieved if the concentration of PPP-TiO_2 NPs exceeds 310 μg/ml and 315 μg/ml, respectively [68].

Details of the application of plant source-mediated nanoparticles in the remediation of wastewater contaminants have been listed in Table 1.

3. Conclusion

The current review addresses the application of nanomaterials contrived from plant-based products as an affordable yet eco-friendly and reproducible strategy for the remediation of heavy metals, organic compounds, dyes, and pathogens from the environment. Their physicochemical properties were identified by drawing on standard laboratory techniques such as TEM, SEM, UV-Vis spectroscopy, XRD, FTIR, SAED, and EDX, among others. Through reduction and absorption mechanisms, the crystalline NPs either independently or in conjunction with other chemicals or reagents removed contaminants within the environment with a certain degree of efficiency depending on the resource used, mode of production, or external parameters such as temperature or pH. Despite their recyclability, rapid reaction time, and high elimination efficiency (~70%), their fragility and susceptibility to ineffectiveness outside of an environment with physically optimum conditions currently restrict any attempts at large-scale commercialization. Nevertheless, with continual advancements in technology and research, the development of feasible protocols for wastewater quality improvement may become plausible.

Data Availability

All relevant data are included within the article.

Conflicts of Interest

All authors declare that there is no conflict of interest.

Acknowledgments

The authors are thankful to their university for providing necessary support for this work.

References

[1] G. A. V. Magalhães-Ghiotto, A. M. de Oliveira, J. P. S. Natal, R. Bergamasco, and R. G. Gomes, "Green nanoparticles in water treatment: a review of research trends, applications, environmental aspects and large-scale production," *Environmental Nanotechnology, Monitoring and Management*, vol. 16, article 100526, 2021.

[2] F. D. Guerra, M. F. Attia, D. C. Whitehead, and F. Alexis, "Nanotechnology for environmental remediation: materials and applications," *Molecules*, vol. 23, no. 7, 2018.

[3] S. Kanchi and S. Ahmed, *Green metal nanoparticles: synthesis, characterization and their applications*, John Wiley & Sons, 2018.

[4] A. G. Ramu, S. Salla, S. Gopi et al., "Surface-tuned hierarchical ϒ-Fe_2O_3-N-rGO nanohydrogel for efficient catalytic removal and electrochemical sensing of toxic nitro compounds," *Chemosphere*, vol. 268, article 128853, 2021.

[5] T. N. V. K. V. Prasad and E. K. Elumalai, "Biofabrication of Ag nanoparticles using _Moringa oleifera_ leaf extract and their antimicrobial activity," *Asian Pacific Journal of Tropical Biomedicine*, vol. 1, no. 6, pp. 439–442, 2011.

[6] M. S. Samuel, E. Selvarajan, T. Mathimani et al., "Green synthesis of cobalt-oxide nanoparticle using jumbo Muscadine (Vitis rotundifolia): Characterization and photo-catalytic activity of acid Blue-74," *Journal of Photochemistry and Photobiology B: Biology*, vol. 211, article 112011, 2020.

[7] S. K. Karupannan, M. J. H. Dowlath, and K. D. Arunachalam, "Phytonanotechnology: challenges and future perspectives," in *In Phytonanotechnology*, pp. 303–322, Elsevier, Netherlands, 2020.

[8] Z. Samadi, K. Yaghmaeian, S. Mortazavi-Derazkola, R. Khosravi, R. Nabizadeh, and M. Alimohammadi, "Facile

green synthesis of zero-valent iron nanoparticles using barberry leaf extract () for photocatalytic reduction of hexavalent chromium," *Bioorganic Chemistry*, vol. 114, article 105051, 2021.

[9] J. Chen, D. Wei, L. Liu et al., "Green synthesis of _Konjac glucomannan_ templated palladium nanoparticles for catalytic reduction of azo compounds and hexavalent chromium," *Materials Chemistry and Physics*, vol. 267, article 124651, 2021.

[10] R. Hao, D. Li, and J. Zhang, "Insights into the removal of Cr(VI) from aqueous solution using plant-mediated biosynthesis of iron nanoparticles," *Environmental Technology and Innovation*, vol. 23, article 101566, 2021.

[11] H. Wang, M. Zhuang, L. Shan et al., "Bimetallic FeNi nanoparticles immobilized by biomass-derived hierarchically porous carbon for efficient removal of Cr(VI) from aqueous solution," *Journal of Hazardous Materials*, vol. 423, article 127098, 2022.

[12] N. El-Desouky, K. R. Shoueir, I. El-Mehasseb, and M. El-Kemary, "Bio-inspired green manufacturing of plasmonic silver nanoparticles/Degussa using Banana waste peduncles: photocatalytic, antimicrobial, and cytotoxicity evaluation," *Journal of Materials Research and Technology*, vol. 10, pp. 671–686, 2021.

[13] E. Ituen, L. Yuanhua, C. Verma, A. Alfantazi, O. Akaranta, and E. E. Ebenso, "Synthesis and characterization of walnut husk extract-silver nanocomposites for removal of heavy metals from petroleum wastewater and its consequences on pipework steel corrosion," *Journal of Molecular Liquids*, vol. 335, article 116132, 2021.

[14] K. M. Al-Qahtani, "Cadmium removal from aqueous solution by green synthesis zero valent silver nanoparticles with _Benjamina_ leaves extract," *Egyptian Journal of Aquatic Research*, vol. 43, no. 4, pp. 269–274, 2017.

[15] Z. Lin, X. Weng, N. I. Khan, G. Owens, and Z. Chen, "Removal mechanism of Sb(III) by a hybrid rGO-Fe/Ni composite prepared by green synthesis via a one-step method," *Science of the Total Environment*, vol. 788, article 147844, 2021.

[16] Y. Peng, M. Azeem, R. Li et al., "Zirconium hydroxide nanoparticle encapsulated magnetic biochar composite derived from rice residue: application for As(III) and As(V) polluted water purification," *Journal of Hazardous Materials*, vol. 423, article 127081, 2022.

[17] R. M. Amin, R. K. Mahmoud, Y. Gadelhak, and F. I. Abo El-Ela, "Gamma irradiated green synthesized zero valent iron nanoparticles as promising antibacterial agents and heavy metal nano-adsorbents," *Environmental Nanotechnology, Monitoring and Management*, vol. 16, p. 100461, 2021.

[18] M. N. Alharthi, I. Ismail, S. Bellucci, and M. A. Salam, "Green synthesis of zinc oxide nanoparticles by _Ziziphus jujuba_ leaves extract: Environmental application, kinetic and thermodynamic studies," *Journal of Physics and Chemistry of Solids*, vol. 158, article 110237, 2021.

[19] K. O. Shittu and O. Ihebunna, "Purification of simulated waste water using green synthesized silver nanoparticles of Piliostigma thonningiiaqueous leave extract," *Advances in Natural Sciences: Nanoscience and Nanotechnology*, vol. 8, no. 4, article 045003, 2017.

[20] G. Sreekala, A. Fathima Beevi, R. Resmi, and B. Beena, "Removal of lead (II) ions from water using copper ferrite nanoparticles synthesized by green method," *Materials Today: Proceedings*, vol. 45, pp. 3986–3990, 2021.

[21] N. Barnawi, S. Allehyani, and R. Seoudi, "Biosynthesis and characterization of gold nanoparticles and its application in eliminating nickel from water," *Journal of Materials Research and Technology*, vol. 17, pp. 537–545, 2022.

[22] S. Altaf, R. Zafar, W. Q. Zaman et al., "Removal of levofloxacin from aqueous solution by green synthesized magnetite (Fe_3O_4) nanoparticles using _Moringa olifera_ : kinetics and reaction mechanism analysis," *Ecotoxicology and Environmental Safety*, vol. 226, article 112826, 2021.

[23] Y. Lin, X. Jin, G. Owens, and Z. Chen, "Simultaneous removal of mixed contaminants triclosan and copper by green synthesized bimetallic iron/nickel nanoparticles," *Science of the Total Environment*, vol. 695, article 133878, 2019.

[24] A. A. Romeh and R. A. Ibrahim Saber, "Green nano-phytoremediation and solubility improving agents for the remediation of chlorfenapyr contaminated soil and water," *Journal of Environmental Management*, vol. 260, p. 110104, 2020.

[25] S. Abbas, S. Nasreen, A. Haroon, and M. A. Ashraf, "Synthesis of silver and copper nanoparticles from plants and application as adsorbents for naphthalene decontamination," *Saudi Journal of Biological Sciences*, vol. 27, no. 4, pp. 1016–1023, 2020.

[26] W. K. Biftu and K. Ravindhranath, "Synthesis of nanoZrO2 via simple new green routes and its effective application as adsorbent in phosphate remediation of water with or without immobilization in Al-alginate beads," *Water Science and Technology*, vol. 81, no. 12, pp. 2617–2633, 2020.

[27] C. Huo, M. Khoshnamvand, P. Liu, C. G. Yuan, and W. Cao, "Eco-friendly approach for biosynthesis of silver nanoparticles using Citrus maxima peel extract and their characterization, catalytic, antioxidant and antimicrobial characteristics," *Materials Research Express*, vol. 6, no. 1, 2019.

[28] M. Nasrollahzadeh, R. Akbari, Z. Issaabadi, and S. M. Sajadi, "Biosynthesis and characterization of Ag/MgO nanocomposite and its catalytic performance in the rapid treatment of environmental contaminants," *Ceramics International*, vol. 46, no. 2, pp. 2093–2101, 2020.

[29] L. Sherin, A. Sohail, M. Mustafa, R. Jabeen, and A. Ul-Hamid, "Facile green synthesis of silver nanoparticles using Terminalia bellerica kernel extract for catalytic reduction of anthropogenic water pollutants," *Colloids and Interface Science Communications*, vol. 37, article 100276, 2020.

[30] A. Makofane, D. E. Motaung, and N. C. Hintsho-Mbita, "Photocatalytic degradation of methylene blue and sulfisoxazole from water using biosynthesized zinc ferrite nanoparticles," *Ceramics International*, vol. 47, no. 16, pp. 22615–22626, 2021.

[31] B. Akilandaeaswari and K. Muthu, "One-pot green synthesis of Au-Ag bimetallic nanoparticles from _Lawsonia inermis_ seed extract and its catalytic reduction of environmental polluted methyl orange and 4-nitrophenol," *Journal of the Taiwan Institute of Chemical Engineers*, vol. 127, pp. 292–301, 2021.

[32] D. Z. Husein, R. Hassanien, and M. F. Al-Hakkani, "Green-synthesized copper nano-adsorbent for the removal of pharmaceutical pollutants from real wastewater samples," *Heliyon*, vol. 5, no. 8, p. e02339, 2019.

[33] K. Sravanthi, D. Ayodhya, and P. Yadgiri Swamy, "Green synthesis, characterization of biomaterial-supported zero-valent iron nanoparticles for contaminated water treatment," *Journal of Analytical Science and Technology*, vol. 9, no. 1, pp. 1–11, 2018.

[34] E. E. Elemike, D. C. Onwudiwe, D. F. Ogeleka, and J. I. Mbonu, "Phyto-assisted preparation of Ag and Ag–CuO nanoparticles using aqueous extracts of Mimosa pigra and their catalytic activities in the degradation of some common pollutants,"

Journal of Inorganic and Organometallic Polymers and Materials, vol. 29, no. 5, pp. 1798–1806, 2019.

[35] G. Manjari, S. Saran, T. Arun, A. V. B. Rao, and S. P. Devipriya, "Catalytic and recyclability properties of phytogenic copper oxide nanoparticles derived from Aglaia elaeagnoidea flower extract," *Journal of Saudi Chemical Society*, vol. 21, no. 5, pp. 610–618, 2017.

[36] P. K. Gautam, S. Shivalkar, and S. Banerjee, "Synthesis of M. oleifera leaf extract capped magnetic nanoparticles for effective lead [Pb (II)] removal from solution: Kinetics, isotherm and reusability study," *Journal of Molecular Liquids*, vol. 305, article 112811, 2020.

[37] D. Chikdu, P. Pal, A. Gujar, R. Deshmukh, and S. Kate, "Green synthesis and characterization of silver nanoparticles by using Aloe barbadensis and its antibacterial activity," *Journal of Global Biosciences*, vol. 4, no. 7, pp. 2713–2719, 2015.

[38] H. B. Slama, A. Chenari Bouket, Z. Pourhassan et al., "Diversity of synthetic dyes from textile industries, discharge impacts and treatment methods," *Applied Sciences*, vol. 11, no. 14, article 6255, 2021.

[39] H. Sadiq, F. Sher, S. Sehar et al., "Green synthesis of ZnO nanoparticles from Syzygium Cumini leaves extract with robust photocatalysis applications," *Journal of Molecular Liquids*, vol. 335, article 116567, 2021.

[40] S. K. Sahoo, G. K. Panigrahi, A. Sahoo, A. K. Pradhan, and A. Dalbehera, "Bio-hydrothermal synthesis of ZnO- $ZnFe_2O_4$ nanoparticles using _Psidium guajava_ leaf extract: role in waste water remediation and plant immunity," *Journal of Cleaner Production*, vol. 318, article 128522, 2021.

[41] M. Rafique, A. J. Shaikh, R. Rasheed et al., "Aquatic biodegradation of methylene blue by copper oxide nanoparticles synthesized from Azadirachta indica leaves extract," *Journal of Inorganic and Organometallic Polymers and Materials*, vol. 28, no. 6, pp. 2455–2462, 2018.

[42] S. Anchan, S. Pai, H. Sridevi, T. Varadavenkatesan, R. Vinayagam, and R. Selvaraj, "Biogenic synthesis of ferric oxide nanoparticles using the leaf extract of _Peltophorum pterocarpum_ and their catalytic dye degradation potential," *Biocatalysis and Agricultural Biotechnology*, vol. 20, article 101251, 2019.

[43] D. Baruah, M. Goswami, R. N. S. Yadav, A. Yadav, and A. M. Das, "Biogenic synthesis of gold nanoparticles and their application in photocatalytic degradation of toxic dyes," *Journal of Photochemistry and Photobiology B: Biology*, vol. 186, pp. 51–58, 2018.

[44] L. Shaker Ardakani, V. Alimardani, A. M. Tamaddon, A. M. Amani, and S. Taghizadeh, "Green synthesis of iron-based nanoparticles using Chlorophytum comosum leaf extract: methyl orange dye degradation and antimicrobial properties," *Heliyon*, vol. 7, no. 2, 2021.

[45] M. Golmohammadi, M. Honarmand, and S. Ghanbari, "A green approach to synthesis of ZnO nanoparticles using jujube fruit extract and their application in photocatalytic degradation of organic dyes," *Spectrochimica Acta - Part A: Molecular and Biomolecular Spectroscopy*, vol. 229, article 117961, 2020.

[46] P. Kumar, M. Govindaraju, S. Senthamilselvi, and K. Premkumar, "Photocatalytic degradation of methyl orange dye using silver (Ag) nanoparticles synthesized from _Ulva lactuca_," *Colloids and Surfaces B: Biointerfaces*, vol. 103, pp. 658–661, 2013.

[47] I. Ali, C. Peng, T. Ye, and I. Naz, "Sorption of cationic malachite green dye on phytogenic magnetic nanoparticles functionalized by 3-marcaptopropanic acid," *RSC Advances*, vol. 8, no. 16, pp. 8878–8897, 2018.

[48] N. Beheshtkhoo, M. A. J. Kouhbanani, A. Savardashtaki, A. M. Amani, and S. Taghizadeh, "Green synthesis of iron oxide nanoparticles by aqueous leaf extract of Daphne mezereum as a novel dye removing material," *Applied Physics A: Materials Science and Processing*, vol. 124, no. 5, pp. 1–7, 2018.

[49] P. Kaur, R. Thakur, H. Malwal, A. Manuja, and A. Chaudhury, "Biosynthesis of biocompatible and recyclable silver/iron and gold/iron core- shell nanoparticles for water purification technology," *Biocatalysis and Agricultural Biotechnology*, vol. 14, pp. 189–197, 2018.

[50] R. Jain, S. Mendiratta, L. Kumar, and A. Srivastava, "Green synthesis of iron nanoparticles using Artocarpus heterophyllus peel extract and their application as a heterogeneous Fenton-like catalyst for the degradation of Fuchsin basic dye," *Current Research in Green and Sustainable Chemistry*, vol. 4, article 100086, 2021.

[51] T. Varadavenkatesan, E. Lyubchik, S. Pai, A. Pugazhendhi, R. Vinayagam, and R. Selvaraj, "Photocatalytic degradation of Rhodamine B by zinc oxide nanoparticles synthesized using the leaf extract of _Cyanometra ramiflora_," *Journal of Photochemistry and Photobiology B: Biology*, vol. 199, article 111621, 2019.

[52] M. A. Ebrahimzadeh, A. Naghizadeh, S. Mohammadi-Aghdam, H. Khojasteh, S. M. Ghoreishi, and S. Mortazavi-Derazkola, "Enhanced catalytic and antibacterial efficiency of biosynthesized _Convolvulus fruticosus_ extract capped gold nanoparticles ()," *Journal of Photochemistry and Photobiology B: Biology*, vol. 209, article 111949, 2020.

[53] A. Ahmed, M. Usman, B. Yu, Y. Shen, and H. Cong, "Sustainable fabrication of hematite (α-Fe_2O_3) nanoparticles using biomolecules of _Punica granatum_ seed extract for unconventional solar-light- driven photocatalytic remediation of organic dyes," *Journal of Molecular Liquids*, vol. 339, article 116729, 2021.

[54] P. Das, S. Ghosh, R. Ghosh, S. Dam, and M. Baskey, "_Madhuca longifolia_ plant mediated green synthesis of cupric oxide nanoparticles: a promising environmentally sustainable material for waste water treatment and efficient antibacterial agent," *Journal of Photochemistry and Photobiology B: Biology*, vol. 189, pp. 66–73, 2018.

[55] F. Bashir, M. Irfan, T. Ahmad et al., "Efficient utilization of low cost agro materials for incorporation of copper nanoparticles to scrutinize their antibacterial properties in drinking water," *Environmental Technology and Innovation*, vol. 21, article 101228, 2021.

[56] R. Balachandar, P. Gurumoorthy, N. Karmegam et al., "Plant-mediated synthesis, characterization and bactericidal potential of emerging silver nanoparticles using stem extract of Phyllanthus pinnatus: a recent advance in phytonanotechnology," *Journal of Cluster Science*, vol. 30, no. 6, pp. 1481–1488, 2019.

[57] V. D. Doan, V. S. Luc, T. L. H. Nguyen, T. D. Nguyen, and T. D. Nguyen, "Utilizing waste corn-cob in biosynthesis of noble metallic nanoparticles for antibacterial effect and catalytic degradation of contaminants," *Environmental Science and Pollution Research*, vol. 27, no. 6, pp. 6148–6162, 2020.

[58] S. Malini, S. Vignesh Kumar, R. Hariharan, A. Pon Bharathi, P. Renuka Devi, and E. Hemananthan, "Antibacterial, photocatalytic and biosorption activity of chitosan nanocapsules embedded with _Prosopis juliflora_ leaf extract synthesized silver nanoparticles," *Materials Today: Proceedings*, vol. 21, pp. 828–832, 2020.

[59] P. P. N. Vijay Kumar, R. L. Kalyani, S. C. Veerla, P. Kollu, U. Shameem, and S. V. N. Pammi, "Biogenic synthesis of stable silver nanoparticles viaAsparagus racemosusroot extract and their antibacterial efficacy towards human and fish bacterial pathogens," *Materials Research Express*, vol. 6, no. 10, article 104008, 2019.

[60] M. Lekeshmanaswamy and K. Anusiyadevi, "Biosynthesis of silver nanoparticles using _Pergularia daemia_ (Hamilton, 1822) leaf extract and its enhanced antibacterial activity against gram negative bacteria _(Escherichia coli)_," *Materials Today: Proceedings*, vol. 48, pp. 201–206, 2022.

[61] W. B. Ayinde, W. M. Gitari, M. Munkombwe, and S. Amidou, "Green synthesis of ag/MgO nanoparticle modified nanohydroxyapatite and its potential for defluoridation and pathogen removal in groundwater," *Physics and Chemistry of the Earth*, vol. 107, pp. 25–37, 2018.

[62] A. Naghizadeh, Z. M. Mizwari, S. M. Ghoreishi, S. Lashgari, S. Mortazavi-Derazkola, and B. Rezaie, "Biogenic and ecobenign synthesis of silver nanoparticles using jujube core extract and its performance in catalytic and pharmaceutical applications: removal of industrial contaminants and in-vitro antibacterial and anticancer activities," *Environmental Technology and Innovation*, vol. 23, article 101560, 2021.

[63] A. T. Babu and R. Antony, "Green synthesis of silver doped nano metal oxides of zinc & copper for antibacterial properties, adsorption, catalytic hydrogenation & photodegradation of aromatics," *Journal of Environmental Chemical Engineering*, vol. 7, no. 1, article 102840, 2019.

[64] T. U. Doan Thi, T. T. Nguyen, Y. D. Thi, K. H. Ta Thi, B. T. Phan, and K. N. Pham, "Green synthesis of ZnO nanoparticles using orange fruit peel extract for antibacterial activities," *RSC Advances*, vol. 10, no. 40, pp. 23899–23907, 2020.

[65] S. Krishnan, S. Murugesan, V. Vasanthakumar et al., "Facile green synthesis of $ZnFe_2O_4$/rGO nanohybrids and evaluation of its photocatalytic degradation of organic pollutant, photo antibacterial and cytotoxicity activities," *Colloids and Surfaces A: Physicochemical and Engineering Aspects*, vol. 611, article 125835, 2021.

[66] P. N. Kirdat, P. B. Dandge, R. M. Hagwane, A. S. Nikam, S. P. Mahadik, and S. T. Jirange, "Synthesis and characterization of ginger (Z. officinale) extract mediated iron oxide nanoparticles and its antibacterial activity," *Materials Today: Proceedings*, vol. 43, pp. 2826–2831, 2021.

[67] A. Dash, M. T. Ahmed, and R. Selvaraj, "Mesoporous magnetite nanoparticles synthesis using the _Peltophorum pterocarpum_ pod extract, their antibacterial efficacy against pathogens and ability to remove a pollutant dye," *Journal of Molecular Structure*, vol. 1178, pp. 268–273, 2019.

[68] M. Abu-Dalo, A. Jaradat, B. A. Albiss, and N. A. F. Al-Rawashdeh, "Green synthesis of TiO_2 NPs/pristine pomegranate peel extract nanocomposite and its antimicrobial activity for water disinfection," *Journal of Environmental Chemical Engineering*, vol. 7, no. 5, article 103370, 2019.

[69] S. Abbas, S. Nasreen, A. Haroon, and M. A. Ashraf, "Synhesis of silver and copper nanoparticles from plants and application as adsorbents for naphthalene decontamination," *Saudi Journal of Biological Sciences*, vol. 27, no. 4, pp. 1016–1023, 2020.

[70] H. M. Mehwish, M. S. R. Rajoka, Y. Xiong et al., "Green synthesis of a silver nanoparticle using Moringa oleifera seed and its applications for antimicrobial and sun-light mediated photocatalytic water detoxification," *Journal of Environmental Chemical Engineering*, vol. 9, no. 4, article 105290, 2021.